Dynamics of an Interhemispheric Teleconnection across the Critical Latitude through a Southerly Duct during Boreal Winter*

SEN ZHAO

State Key Laboratory of Numerical Modeling for Atmospheric Sciences and Geophysical Fluid Dynamics, Institute of Atmospheric Physics, Chinese Academy of Sciences, and University of Chinese Academy of Sciences, Beijing, China

JIANPING LI

College of Global Change and Earth System Science (GCESS), Beijing Normal University, and Joint Center for Global Change Studies, Beijing, China

YANJIE LI

State Key Laboratory of Numerical Modeling for Atmospheric Sciences and Geophysical Fluid Dynamics, Institute of Atmospheric Physics, Chinese Academy of Sciences, Beijing, China

(Manuscript received 15 June 2014, in final form 8 May 2015)

ABSTRACT

In this study, an interhemispheric teleconnection pattern across the critical latitude from southern Africa through South Asia to the North Pacific was revealed in boreal winter monthly averaged 250-hPa streamfunction fields obtained from both the 40-yr ECMWF Re-Analysis (ERA-40) and the NCEP–NCAR reanalysis data from 1957/58 to 2001/02. Classical Rossby wave theory for zonally varying flow in which the effects of the basic-state meridional wind are ignored predicts that stationary Rossby waves cannot propagate across easterlies. To elucidate the underlying mechanisms responsible for this interhemispheric teleconnection, the theoretical basis for stationary wave propagation across the critical latitude is considered, taking into account meridional ambient flow. The theoretical results suggest that the southerly flow over East Africa, the western Indian Ocean, and South Asia creates a path for the northward propagation of stationary waves across the critical latitude. Stationary wavenumber and group velocity analysis, ray tracing, and simple model experiments applied to nearly realistic boreal winter mean flows confirm that disturbances excited in southern Africa and the western Indian Ocean can propagate across the critical latitude to South Asia through the southerly duct and then continue downstream along the North African–Asian subtropical jet.

1. Introduction

Interhemispheric atmospheric teleconnections have recently received considerable attention, primarily because the information emanating from one hemisphere is considered a potential source of improvement for predictions in the other. Many studies have documented the connection between the hemispheres in terms of climate conditions and forcing. For instance, Lin (2009) and Lee et al. (2013) reported the southern atmospheric response to diabatic heating of the northern summer monsoons. Wang et al. (2010) and Ji et al. (2014) demonstrated the interhemispheric influence of the anomalous Atlantic warm pool on the southeastern Pacific, and considerable evidence indicates an influence of the Southern Hemisphere (SH) annular mode on the Northern Hemisphere (NH) climate (e.g., Nan and Li 2003; Nan et al. 2009; Song et al. 2009; Wu et al. 2009; Zheng et al. 2013). There are,

Denotes Open Access content.

* Supplemental information related to this paper is available at the Journals Online website: http://dx.doi.org/10.1175/JCLI-D-14-00425.s1.

Corresponding author address: Prof. Jianping Li, College of Global Change and Earth System Science (GCESS), Beijing Normal University, No.19 Xinjiekouwai St., Beijing 100875, China. E-mail: ljp@bnu.edu.cn

DOI: 10.1175/JCLI-D-14-00425.1

however, also situations when disturbances from a tropical source affect both hemispheres, thus producing covariability between regions in the two hemispheres. Specific examples include the interhemispheric symmetries of Pacific climate that are influenced by the interannual El Niño–Southern Oscillation (ENSO) and decadal ENSO-like variations (Dettinger et al. 2001), and also the interhemispheric dipole between the subtropical region in the western Pacific and the region east of Australia produced by intraseasonal tropical convection during the boreal summer (Hines and Bromwich 2002; Liu et al. 2010).

Teleconnection patterns in the atmosphere are caused by energy transport and wave propagation (e.g., Frederiksen and Webster 1988; Trenberth et al. 1998; Liu and Alexander 2007), where the wave propagation depends on background flow. Since the pioneering work of Rossby (1939) and Yeh (1949), who examined Rossby wave propagation on a constant background flow, considerable effort has been devoted to understanding Rossby wave propagation through spatially varying background flows. Hoskins and Karoly (1981, hereinafter HK) demonstrated the meridional propagation of stationary waves from the tropics to midlatitudes on zonally symmetric zonal flows (ZSZF). However, HK's theory suggests that the interhemispheric linkages above should not occur at the critical latitude (i.e., the latitude where the zonal wind is equal to zero) in the upper-tropospheric state that acts as a barrier to stationary waves.

Extension of the Rossby wave theory to asymmetric basic states indicates that such interhemispheric connections are possible. One such mechanism, which was identified from model simulations by Webster and Holton (1982), is the "westerly duct." These authors suggest that while the mean zonal wind is easterly at low latitudes, there are zones of time-mean westerlies in the equatorial upper troposphere. In these westerly ducts, stationary waves can propagate across the equator and interhemispheric interactions may occur. Subsequent studies have reported analytical and observational data regarding this mechanism. Karoly (1983) extended Rossby wave ray tracing theory to a latitudinally and longitudinally varying basic state with both zonal and meridional components [herein referred to as horizontally nonuniform flow (HNF)]. Hoskins and Ambrizzi (1993, hereinafter HA) suggested that HK's stationary wavenumber theory could be applied to a longitudinally varying zonal flow [herein referred to as zonally varying zonal flow (ZVZF)] by considering the local latitudinal zonal wind profile in the basic state. Karoly's (1983) ray tracings and HA's stationary wavenumber analysis are in agreement with the wavelike disturbances observed in the equatorial east Pacific (Hsu and Lin 1992; Kiladis and Weickmann 1992; Tomas and Webster 1994; Knippertz 2007). From a nonstationary wave perspective, many studies (Karoly 1983; Li and Nathan 1994, 1997; Yang and Hoskins 1996) have also shown that negative-frequency Rossby waves (corresponding to westward movement) can propagate through the tropical easterlies into the extratropics for both zonally uniform and zonally varying basic states.

However, few of the above studies of asymmetric basic states considered the influence of the meridional basic flow on stationary Rossby wave propagation. Schneider and Watterson (1984) and Li and Li (2012) demonstrated that zonally uniform meridional flow (mean meridional circulation) can create the one-way transmission of waves across the critical latitude in the direction of the meridional flow. Kraucunas and Hartmann (2007) also explored the roles of mean meridional winds in promoting the propagation of wave activity across the equator, using a nonlinear shallow-water model. Wang et al. (2005) showed that a southerly flow component in an idealized basic state may enable the transfer of a Rossby wave northward from tropical easterlies into extratropical westerlies and thus excite a response in the extratropics. However, it is unclear how a meridional flow including zonal variations, especially a more realistic climatological flow, affects the wave propagation behavior near the critical latitude.

The aim of this study is to examine possible interhemispheric propagation within a realistic climatological flow. To determine the significance of wave propagation across easterlies for the real atmosphere, it is natural to extend previous investigations of teleconnections by seeking an interhemispheric pattern that crosses the critical latitude. If such a pattern exists, it is important to consider whether it can be explained by stationary wave energy propagation across the critical latitude in a southerly or northerly duct. This topic is the focus of this study.

The remainder of this paper is organized as follows. In section 2, we present the datasets, methods of analysis, and model used in the research. In section 3, we examine the existence of low-frequency teleconnections through easterlies in the boreal winter. To confirm that such a teleconnection pattern is consistent with Rossby wave propagation, a brief review of stationary wave horizontal propagation theory is given in section 4. New understandings of the relationships between ambient flow and group velocity around the critical latitudes are discussed in detail. In section 5, stationary wavenumber and group velocity analysis, as well as wave ray tracing techniques, are applied to a nearly realistic background flow to verify the evidence for interhemispheric propagation of stationary Rossby waves across the easterlies through a southerly duct. Further simple barotropic model experiments are used to confirm the above results. Finally, a summary and discussion are presented in section 6.

2. Data, analysis methods, and model

a. Data and analysis methods

Previous studies have detected atmospheric teleconnections using upper-tropospheric variables such as geopotential height (e.g., Wallace and Gutzler 1981), streamfunction (Hsu and Lin 1992; Branstator 2002), and meridional velocity (Lu et al. 2002). Geopotential height emphasizes the disturbances at higher latitudes but is not appropriate for depicting teleconnection patterns at low latitudes because of its weaker variability there and the invalidity of the quasigeostrophic approximation (Hsu and Lin 1992; Branstator 2002). Compared with geopotential height and streamfunction, meridional velocity is less influenced by meridional shifts of the jet stream; hence, the teleconnection patterns of meridional velocity are more zonally oriented (Lu et al. 2002). Therefore, the streamfunction field is chosen to analyze low-frequency teleconnections in the present study, because this paper focuses on investigating interhemispheric behavior in the vicinity of easterlies in the tropics.

The datasets used in this study include monthly data from the 40-yr European Centre for Medium-Range Weather Forecasts (ECMWF) Re-Analysis (ERA-40; Uppala et al. 2005; ECMWF 2005) and from the National Centers for Environmental Prediction–National Center for Atmospheric Research (NCEP–NCAR) reanalysis (Kalnay et al. 1996; NCEP 1996) for the common period 1957–2002. Monthly mean rainfall from the National Oceanic and Atmospheric Administration (NOAA) Climate Prediction Center (CPC) Merged Analysis of Precipitation (CMAP; Xie and Arkin 1997; CPC 1995) and NOAA interpolated outgoing longwave radiation (OLR; Liebmann and Smith 1996; CPC 1996) during 1979–2002 are analyzed as proxies for convective activity and diabatic heating, respectively. Several teleconnection indices are used: the Eurasian (EU), the Pacific–North American (PNA), the western Pacific (WP), and the southern Eurasian (SEA). The EU, PNA, and WP indices are based on centers of action of 500-hPa height patterns, as defined by Wallace and Gutzler (1981), and the SEA is based on centers of action of 250-hPa height patterns, as defined by Xu (2013). The Niño-3 index, obtained from the Climate Prediction Center (CPC 2011), is used to quantify ENSO.

The streamfunction was calculated from relative vorticity by inverting the Laplacian operator in spherical harmonic space. Following Branstator (2002), we use monthly mean departures from centered 3-month averages when analyzing the streamfunction field. By doing this, much of the influence of interannual SST and trends has been removed, and we can obtain larger samples than if we used seasonal means. The out-of-phase relationship between the NH and SH appears to dominate the one-point correlation maps for the streamfunction fields, indicating the existence of a strong zonal mean component (Branstator 1990; Hsu and Lin 1992). The eddy streamfunction was calculated by subtracting the zonal mean component to reveal the Rossby wave characteristics of large-scale circulation. To focus on large-scale features, we also applied a horizontal smoothing to rainfall and OLR by multiplying a spherical harmonic component with total wavenumber n by $\exp\{-\xi[n(n+1)]^2\}$, where the coefficient ξ has been set such that the harmonic component of $n = 48$ is reduced by 37%.

The teleconnectivity technique (Wallace and Gutzler 1981) is applied to the eddy streamfunction field to reveal the teleconnection structure at low latitudes. The teleconnectivity is defined as $T_i = |(r_{ij})\text{minimum for all } j|$, where r_{ij} is the correlation between point i and any point j. This is an efficient method for detecting standing oscillations and has been used previously (e.g., Hsu and Lin 1992; Ambrizzi et al. 1995).

b. Barotropic model

The barotropic model used in this study is based on the damped barotropic vorticity equation linearized about the HNF:

$$\left(\frac{\partial}{\partial t}+\frac{\overline{u}}{a\cos\varphi}\frac{\partial}{\partial\lambda}+\frac{\overline{v}}{a}\frac{\partial}{\partial\varphi}\right)\nabla^2\psi'+J(\psi',\overline{\zeta}+f)$$
$$=S'-\alpha\nabla^2\psi'-K\nabla^4(\nabla^2\psi'), \tag{1}$$

where (u, v) are the horizontal components of wind; ψ is the streamfunction; ζ is the relative vorticity; f is the Coriolis parameter; λ and φ are longitude and latitude; and a is the radius of the earth; primes and overbars denote the perturbation and basic states, respectively. The model has a T42 spectral horizontal resolution with a linear damping rate of $(10\text{ day})^{-1}$ ($\alpha = 1.16\times10^{-6}\,\text{s}^{-1}$). The value of the diffusion coefficient is $K = 2.34\times10^{-16}\,\text{m}^4\,\text{s}^{-1}$, as used by Branstator (1983) to investigate the propagation of energy in a barotropic atmosphere. The vorticity forcing term S' takes the same elliptical form as in Wang et al. (2005):

$$S'=\begin{cases}S_0\left\{1-\left[\dfrac{(\lambda-\lambda_0)^2}{\lambda_d^2}+\dfrac{(\varphi-\varphi_0)^2}{\varphi_d^2}\right]\right\}, & \text{for } \left[\dfrac{(\lambda-\lambda_0)^2}{\lambda_d^2}+\dfrac{(\varphi-\varphi_0)^2}{\varphi_d^2}\right]\le 1\\ 0, & \text{otherwise}\end{cases}, \tag{2}$$

where $S_0 = 1.16 \times 10^{-10}$, (λ_0, φ_0) denotes the forcing center, and λ_d and φ_d are the zonal and meridional extents of the forcing, respectively. The values $\lambda_d = 12°$ and $\varphi_d = 7°$ are applied in this calculation. Equation (1) is numerically integrated with a fourth-order Runge–Kutta scheme. The steady response of the model is obtained at 25 days, when the solution has reached a steady state.

3. Interhemispheric teleconnection pattern

Figure 1 shows the teleconnectivity of the monthly mean winter [December–February (DJF)] eddy streamfunction at 250 hPa. The grid points connected by arrows exhibit the strongest negative correlations on their one-point correlation plots. Figure 1 shows a well-defined interhemispheric link across the critical latitude, with one pole in southern Africa (5°S, 27.5°E) and the other in South Asia (17.5°N, 65°E). The one-point correlation plots for these two locations are shown in Fig. 2. The two correlation plots show quadrupole large-scale anomalies with centers in southern Africa, South Asia, the tropical North Pacific, and the tropical South Pacific, together with an arc-like wave pattern extending from the central North Pacific to the North American region. Similar results were also derived by applying the same technique to NCEP–NCAR reanalysis data (see Figs. S1 and S2 in the supplemental material). These results indicate that interhemispheric links across the critical latitude are apparent in the boreal winter.

The arc-like wave patterns in the North Pacific are significant for both base points, whereas there are either no distinct, or very weak, extratropical signals in the SH (Figs. 2a,b). Examination of other one-point correlation maps for a set of base points near 5°S, 27.5°E and 17.5°N, 65°E shows similar extratropical patterns to those in Fig. 2, indicating that the disturbance energy preferentially propagates to the NH rather than the SH. This hypothesis is further explored in section 5.

To identify this interhemispheric pattern more clearly, the southern Africa–South Asia–North Pacific (AAP) index (AAPI) is defined as

$$\mathrm{AAPI} = \psi'^*(5°\mathrm{S}, 27.5°\mathrm{E}) - \psi'^*(17.5°\mathrm{N}, 65°\mathrm{E}), \quad (3)$$

where ψ'^* denotes the eddy streamfunction anomalies. Here, we use only the base points in southern Africa and South Asia, rather than that in the Pacific, to avoid including the effects of other teleconnections. To further distinguish the AAP teleconnection pattern from classical teleconnections, we remove variability associated with well-known teleconnection indices and the ENSO index via multiple regression. After removal of the contributions of the SEA, EU, PNA, WP, and ENSO,

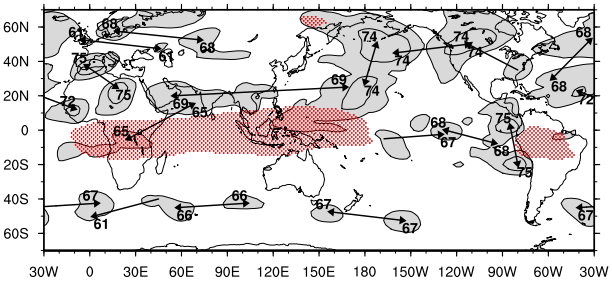

FIG. 1. Teleconnectivity of monthly mean DJF eddy streamfunction departures from centered 3-month averages at 250 hPa during the period 1958/59–2001/02 based on ERA-40. All correlation coefficients have been multiplied by 100. Values < 60 are not contoured and the contour interval is 10. Values at the local maxima are shown. The grid points connected by arrows exhibit the strongest negative correlations on their one-point correlation maps. The red dotted regions denote climatological easterlies.

the major circulation features (Fig. 3) resemble those in Fig. 2a, indicating that the AAP is independent of these traditional teleconnections and is not forced by ENSO.

The obvious teleconnectivity (Fig. 1) and small-scale standing anomalies (Fig. 3) in the eastern equatorial Pacific may correspond to cross-equatorial wave propagation in the westerly duct. This interhemispheric link has been well documented in previous studies (e.g., Webster and Holton 1982; Tomas and Webster 1994). However, the interhemispheric link across the critical latitude has received less attention. In the following sections, we provide a theoretical explanation of the AAP interhemispheric link in terms of stationary wave propagation on HNF.

4. Theoretical basis for stationary Rossby wave propagation

a. Zonally varying zonal flow

We begin by reviewing the classical theory for the basic state on ZSZF (HK) and an extension to ZVZF (HA). The nondivergent barotropic vorticity equation linearized about $\overline{u} = \overline{u}(y)$ on a Mercator projection of a sphere takes the form

$$\left(\frac{\partial}{\partial t} + \overline{u}_M \frac{\partial}{\partial x}\right)\nabla_M^2 \psi' + \overline{\beta}_M \frac{\partial \psi'}{\partial x} = 0, \quad (4)$$

where $\overline{u}_M = \overline{u}/\cos\varphi$ is the ambient zonal wind and

$$\overline{\beta}_M = \frac{2\Omega\cos^2\varphi}{a} - \frac{\cos\varphi}{a^2}\frac{d}{d\varphi}\left[\frac{1}{\cos\varphi}\frac{d}{d\varphi}(\overline{u}\cos\varphi)\right] \quad (5)$$

is the meridional gradient of the absolute vorticity in the Mercator projection. The dispersion relation for free plane wave solutions $\exp[i(kx + ly - \omega t)]$ superimposed

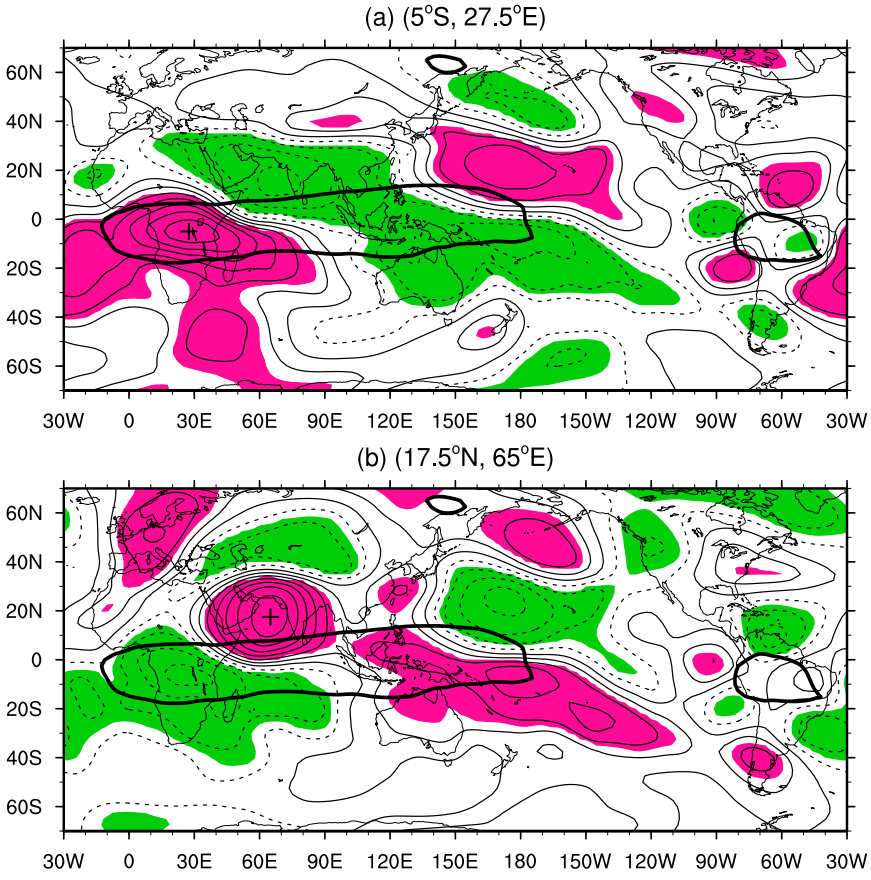

FIG. 2. One-point correlation plots of monthly mean DJF eddy streamfunction departures from centered 3-month averages at 250 hPa derived from the ERA-40. The base points are marked by a + sign and with coordinates listed at the top of each plot: (a) 5°S–27.5°E and (b) 17.5°N–65.0°E. The contour interval is 0.15 and negative contours are dashed. The shaded areas indicate significance at the 99% confidence level (Student's t test). Thick black curves denote the climatological zero zonal wind line.

on $\overline{u}_M$ and $\overline{\beta}_M$ that vary slowly enough with latitude for the WKBJ approximation to be valid, is

$$\omega = \overline{u}_M k - \frac{\overline{\beta}_M k}{K^2}, \tag{6}$$

where ω is the frequency of the disturbances; k and l are zonal and meridional wavenumbers, respectively; and K is the total wavenumber, defined by $K^2 = k^2 + l^2$. The latitudinal distribution of the meridional wavenumber l can be calculated for a given zonal wavenumber k for the stationary wave ($\omega = 0$), yielding

$$l^2(\varphi) = K_s^2 - k^2, \tag{7}$$

where K_s^2 is the stationary wavenumber, defined as

$$K_s^2(\varphi) \equiv \frac{\overline{\beta}_M}{\overline{u}_M}. \tag{8}$$

The stationary waves can propagate if the flow is westerly ($\overline{u}_M$ positive) with positive meridional absolute vorticity gradient ($\overline{\beta}_M$ positive). The case with easterly flow and negative $\overline{\beta}_M$ is usually not considered, since it is rare in the real atmosphere.

HA suggested that the theory of Eqs. (6) and (8) for zonally averaged flow can be applied to a realistic longitudinally varying flow by considering the local latitudinal zonal wind profile; that is, by replacing $\overline{u}_M(\varphi)$ and $\overline{\beta}_M(\varphi)$ in Eq. (8) with the local flow state $\overline{u}_M(\lambda, \varphi)$ and $\overline{\beta}_M(\lambda, \varphi)$ separately to obtain the local stationary wavenumber $K_s(\lambda, \varphi)$. This extension is based on the assumptions that 1) meridional flow and the zonal absolute vorticity gradient may be neglected to a first-order approximation compared with zonal flow and the meridional absolute vorticity gradient, respectively; and 2) the meridional wavelength is greater than or equal to the zonal wavelength. As shown by HA, the waves are

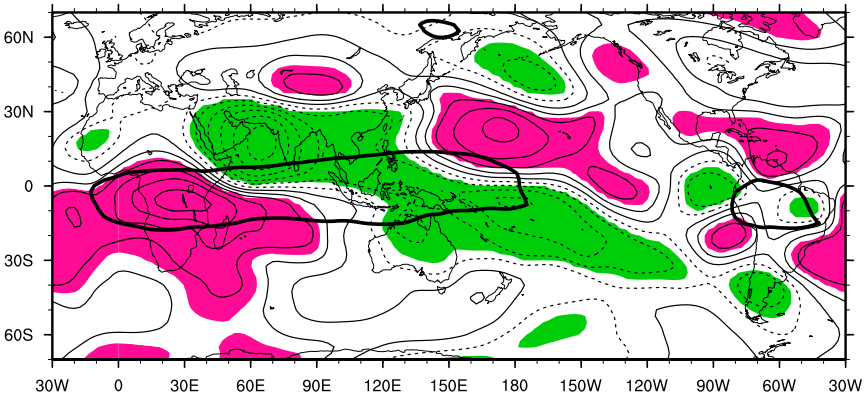

FIG. 3. As in Fig. 2a, but for eddy streamfunction departures from centered 3-month averages against the AAPI after removal of the contributions of SEA, EU, PNA, and WP teleconnections and ENSO.

trapped in a region with a latitudinal maximum of K_s that is flanked by lower values that often occur around the strong westerly jets; the waves also tend to propagate toward higher values of K_s, and they reflect from a turning latitude ($K_s = k$ and $l = 0$). HA's theory is a useful theoretical basis for the teleconnection behavior in observations and models. Examples include chains of highs and lows meridionally trapped along the jet stream (e.g., Ambrizzi et al. 1995; Branstator 2002; Lu et al. 2002; Enomoto et al. 2003; Ding and Wang 2005) and cross-equatorial propagation of waves in the westerly duct in the tropics (e.g., Hsu and Lin 1992; Kiladis and Weickmann 1992; Tomas and Webster 1994; Knippertz 2007). However, at the critical latitude ($\overline{u}_M = 0$), the wave may break, with the meridional scale and group velocity tending to zero. Hence, the stationary wave cannot propagate through the critical latitude from the tropical easterlies to the extratropics on a basic state with meridional flow neglected.

b. *Horizontally nonuniform flow*

The dispersion relationship for barotropic Rossby plane wave propagation on an HNF that includes a meridional component (e.g., Karoly 1983; Li and Li 2012) can be written as

$$\omega = \overline{u}_M k + \overline{v}_M l + \frac{\overline{q}_x l - \overline{q}_y k}{K^2}, \tag{9}$$

where $(\overline{u}_M, \overline{v}_M) = (\overline{u}, \overline{v})/\cos\varphi$ is the ambient velocity on a Mercator projection, and the zonal and meridional gradients of absolute vorticity—$\overline{q}_x$, and $\overline{q}_y$, respectively—take the forms

$$\overline{q}_x = \frac{1}{a^2\cos\varphi}\left(\frac{\partial^2\overline{v}}{\partial\lambda^2} - \frac{\partial^2\overline{u}}{\partial\varphi\partial\lambda}\cos\varphi + \frac{\partial\overline{u}}{\partial\lambda}\sin\varphi\right) \tag{10a}$$

and

$$\overline{q}_y = \overline{\beta}_M + \frac{\partial^2\overline{v}}{\partial\varphi\partial\lambda} + \tan\varphi\frac{\partial\overline{v}}{\partial\lambda}. \tag{10b}$$

From Eq. (9), the group velocity vector $\mathbf{c}_g = (u_g, v_g) = (\partial\omega/\partial k, \partial\omega/\partial l)$ takes the form

$$u_g = \overline{u}_M + [(k^2 - l^2)\overline{q}_y - 2kl\overline{q}_x]/K^4 \tag{11a}$$

and

$$v_g = \overline{v}_M + [2kl\overline{q}_y + (k^2 - l^2)\overline{q}_x]/K^4. \tag{11b}$$

The energy conveyed by Rossby waves propagates with the group velocity. Following Lighthill (1978), the wave ray is defined as a trajectory that is locally tangential to the group velocity. The wavenumbers k and l, which vary along the ray, can be found from kinematic wave theory (Whitham 1960) as

$$\frac{D_g k}{Dt} = -k\frac{\partial\overline{u}_M}{\partial x} - l\frac{\partial\overline{v}_M}{\partial x} + \frac{\overline{q}_{yx}k - \overline{q}_{xx}l}{K^2} \quad \text{and} \tag{12a}$$

$$\frac{D_g l}{Dt} = -k\frac{\partial\overline{u}_M}{\partial y} - l\frac{\partial\overline{v}_M}{\partial y} + \frac{\overline{q}_{yy}k - \overline{q}_{xy}l}{K^2}, \tag{12b}$$

where $D_g/Dt = \partial/\partial t + \mathbf{c}_g \cdot \nabla_M$ represents the material derivative along the ray, and the second x and y subscripts denote the partial derivatives with respect to that subscript. The zonal wavenumber k along the ray is not constant, as a result of zonal variations in the basic state.

To further explore the propagating behavior on HNF, Eq. (9) can be rewritten in terms of a cubic polynomial of l (Li and Li 2012) as

$$f(l) = \overline{v}_M l^3 + k(\overline{u}_M - c)l^2 + (k^2\overline{v}_M + \overline{q}_x)l + [k^2(\overline{u}_M - c) - \overline{q}_y]k = 0, \quad (13)$$

where c is the zonal phase velocity, defined as $c = \omega/k$. Stationary waves ($c = 0$) are assumed in the following, and nonstationary waves ($c \neq 0$) may be extended by substituting $\overline{u}_M - c$ for $\overline{u}_M$.

When meridional flow is excluded from the basic state ($\overline{v}_M \equiv 0$), Eq. (10b) shows that $\overline{q}_y$ can be simplified to Eq. (5). Similarly, from Eq. (10a) $\overline{q}_x$ is zero since the basic state is nondivergent. Therefore, Eq. (13) reduces to the classical Rossby wave dispersion relationship, as in Eq. (7). This suggests that classical Rossby theory on ZSZF is a specific case of that on HNF.

The propagation behavior changes dynamically with the inclusion of the meridional flow in the basic state. For $\overline{v}_M \neq 0$, the cubic Eq. (13) has either one or three real roots because the complex conjugate roots are always coupled. In the case of three real roots, Eq. (13) must have two extrema with opposite signs for real l, l_1 and l_2, where the partial derivative $\partial f/\partial l$ is zero. The extrema l_1 and l_2 of $f(l)$ can be expressed as

$$l_{1,2} = k\frac{-\overline{u}_M \pm [\overline{u}_M^2 - 3\overline{v}_M(\overline{v}_M + \overline{q}_x/k^2)]^{1/2}}{3\overline{v}_M}.$$

Hence, the sufficient conditions for the existence of three real (propagating) roots can be written as

$$\begin{cases} \overline{u}_M^2 > 3\overline{v}_M(\overline{v}_M + \overline{q}_x/k^2) \\ f(l_1)f(l_2) < 0 \end{cases}, \quad (14)$$

If Eq. (14) is violated, Eq. (13) has one real (propagating) root, and the other two are complex conjugate (evanescent) roots. A version of Eq. (13) was discussed by Opsteegh (1982) and Schneider and Watterson (1984), but they failed to consider the zonal variations of the basic flow. Consequently, unlike Eq. (14), Schneider and Watterson's (1984) condition for three propagating solutions [Eq. (17)] is independent of the zonal wavelength and zonal flow variations.

At a critical latitude ($\overline{u}_M = 0$), Eq. (13) can be expressed as

$$\overline{v}_M l^3 + (k^2\overline{v}_M + \overline{q}_x)l - \overline{q}_y k = 0. \quad (15)$$

The propagation behaviors of the four possible local basic-state situations at a critical latitude can be summarized as follows:

(i) When the local basic state satisfies $\overline{v}_M \neq 0$ and $\overline{q}_y > 0$, Eq. (14) is violated, indicating there is only one propagating root and two complex conjugate roots in this case. Because the product of the roots of cubic Eq. (15) is $\overline{q}_y k/\overline{v}_M$, the propagating root can be expressed as

$$l = \frac{1}{C}\frac{\overline{q}_y k}{\overline{v}_M}, \quad (16)$$

where C is the product of the two complex conjugate roots and, hence, is always positive. Then the local meridional wavenumber has the same sign as $\overline{v}_M$; consequently, for $\overline{v}_M > 0$, the isophase lines of the wave solution are oriented southeast–northwest, but for $\overline{v}_M < 0$ they are oriented southwest–northeast. If $\overline{q}_x$ is negligible compared with $\overline{q}_y$, the term that involves $\overline{q}_x$ can be neglected in Eq. (11b). Then, substituting Eq. (16) into Eq. (11b), the meridional group velocity takes the form

$$v_g = \frac{1}{\overline{v}_M}\left(\overline{v}_M^2 + \frac{1}{C}\frac{2k^2\overline{q}_y^2}{K^4}\right). \quad (17)$$

Eq. (17) shows that the meridional component of group velocity v_g must be in the same direction as $\overline{v}_M$, indicating that a northerly (southerly) ambient flow favors southward (northward) energy propagation across the critical latitude.

(ii) The case that $\overline{v}_M \neq 0$ and $\overline{q}_y < 0$ usually occurs to the south or north of a strong jet with a large meridional gradient of zonal wind. A similar analysis to that applied in case (i) shows that, for $\overline{q}_y < 0$, the local meridional wavenumber of the propagating root has the opposite sign to $\overline{v}_M$, while the corresponding v_g has the same sign as $\overline{v}_M$.

(iii) In the case of $\overline{v}_M \neq 0$ and $\overline{q}_y = 0$, if $k^2 + \overline{q}_x/\overline{v}_M > 0$, then Eq. (15) has two propagating roots. For example, with $\overline{q}_x \sim 10^{-12}\,\mathrm{m^{-1}\,s^{-1}}$ and $\overline{v}_M \sim 1\,\mathrm{m\,s^{-1}}$, real roots exist for approximately $k > 6$. However, if $k^2 + \overline{q}_x/\overline{v}_M \leq 0$, roots appear as complex conjugate pairs (evanescent) or $l = 0$ (invalid for the WKBJ approximation as the wave scale becomes too large).

(iv) When $\overline{v}_M = 0$, Eq. (15) reduces to a linear equation for l. If $\overline{q}_x \neq 0$, the wave can tunnel across the critical latitude with local meridional wavenumber root $l = \overline{q}_y k/\overline{q}_x$. As $\overline{q}_x \to 0$ (similar to HA's assumption on the ZVZF), the root has $|l| \to \infty$, indicating that the meridional wavelength approaches zero and the waves cannot propagate through the critical latitude. This is rare and usually occurs only at isolated points in the real atmosphere.

It is important to note that local nonzero meridional flow may create a duct for stationary wave one-way propagation across the critical latitude. Moreover, the

wave energy always disperses in the same direction as the local meridional basic flow if $\overline{q}_x$ is negligible compared with $\overline{q}_y$, which is generally the case in the atmosphere. The propagation mechanism is different from that proposed by Schneider and Watterson (1984) since it includes the effects of zonal variations in the basic-state meridional wind. Although the zonal mean meridional winds are southerlies in the tropical easterlies (e.g., the boreal winter upper-tropospheric winds), the meridional basic winds also vary longitudinally; that is, the meridional flows are southerlies in particular geographical domains but northerlies elsewhere. In these southerly ducts, northward energy propagation of stationary waves across the critical latitude is possible, and southward energy propagation is suppressed, and vice versa in the northerly ducts, where southward energy propagation of stationary waves across the critical latitude is possible and northward energy propagation is suppressed.

5. Stationary wave propagation around the critical latitude in the DJF climatological flow

The theoretical analysis described above indicates that the inclusion of meridional flow in the basic state can enable stationary Rossby wave propagation across the easterlies, which may help explain the observed AAP teleconnection in the boreal winter. To test this hypothesis and to further explore which of the processes in the full theory contribute to the meridional propagation through regions of easterlies, we performed propagating stationary wavenumber and group velocity analysis, ray tracing analysis, and simple model experiments using a barotropic model with approximately realistic DJF 250-hPa climatological flow.

a. *Basic flow*

The WKBJ approximation for Rossby wave propagation on realistic flows requires the basic state to vary slowly compared with the disturbance field (Li and Nathan 1997). For this reason, the observed DJF mean ambient winds were smoothed using a two-dimensional Fourier series, and truncated at zonal wavenumber 5 and meridional wavenumber 8 to remove the small-scale signals in the basic state. In one dimension, the WKBJ approximate solution is valid provided that

$$|dl^{-1}/dy| < 1; \tag{18}$$

that is, provided the length scale l^{-1} is slowly varying (HK). HK proved that $l^{-1/2}$ is approximately equivalent to the wave amplitude. The WKBJ criterion Eq. (18) is satisfied in the zonal band range from 55°S to 75°N for the smoothed zonal averaged flow (see Fig. S3 in the supplemental material), indicating that the WKBJ solution is valid for interhemispheric propagation on ZSZF. However, the extension of the WKBJ criterion to two dimensions is not as simple, as we cannot express the wave amplitude in terms of wavenumber explicitly. One may obtain a set of necessary conditions by applying Eq. (18) locally to the meridional direction on ZVZF following HA. The WKBJ criterion for the smoothed flow satisfies almost all instances where HA's theory predicts that stationary waves are able to propagate (see Fig. S4 in the supplemental material). This suggests WKBJ analysis is feasible for the smoothed 2D zonal flow. As no such WKBJ criterion existed for HNF until now, the validity of the solution has yet to be quantitatively tested. Despite this, the WKBJ solution will provide qualitative information on the propagation behavior of Rossby waves through comparison with barotropic model solutions.

During the boreal winter, easterly winds prevail over the tropical regions, except for relatively weak westerlies in the tropical east Pacific and tropical Atlantic (Fig. 4a). Northerly winds dominate regions of easterlies in the Eastern Hemisphere (EH), with an amplitude of about $3\,\mathrm{m\,s^{-1}}$, which is considerable compared with the zonal winds in this region (Fig. 4b). The North African–Asian jet and the North American jet are strong and produce strong positive $\overline{q}_y$ along the jet and are flanked by negative values (Fig. 4c). Compared with $\overline{q}_y$, $\overline{q}_x$ is weak, with an amplitude of only about one-tenth of $\overline{q}_y$ for most areas (Fig. 4d).

To address the importance of meridional basic flow for the meridional propagation of stationary waves, we considered three basic-state situations: (i) ZVZF, which is a purely zonal flow without the meridional flow component [i.e., $\overline{u}_M = \overline{u}_M(\lambda, \varphi)$, $\overline{v}_M = 0$, $\overline{q}_y = \overline{\beta}_M(\lambda, \varphi)$, and $\overline{q}_x = 0$, corresponding to HA's theory]; (ii) partial HNF (PHNF), which includes the meridional flow but ignores $\overline{q}_x$ and variations in the meridional flow in $\overline{q}_y$ for comparison with HA's theory [i.e., $\overline{u}_M = \overline{u}_M(\lambda, \varphi)$, $\overline{v}_M = \overline{v}_M(\lambda, \varphi)$, $\overline{q}_y = \overline{\beta}_M(\lambda, \varphi)$, and $\overline{q}_x = 0$; this case is also identical to the basic state used by Schneider and Watterson (1984), if applied locally]; and (iii) fully HNF (FHNF), where full variations of basic flow are considered [i.e., $\overline{u}_M = \overline{u}_M(\lambda, \varphi)$, $\overline{v}_M = \overline{v}_M(\lambda, \varphi)$, $\overline{q}_y = \overline{q}_y(\lambda, \varphi)$, and $\overline{q}_x = \overline{q}_x(\lambda, \varphi)$].

b. *Meridional wavenumber and group velocity of propagating stationary waves*

The solutions for the dispersion relationship [Eq. (13)] with real meridional wavenumbers represent propagating waves. The sign of the meridional wavenumber governs the direction perpendicular to isophase lines, whereas the corresponding meridional group velocity gives the north–south direction of energy propagation. These properties are widely used as proxies for identifying

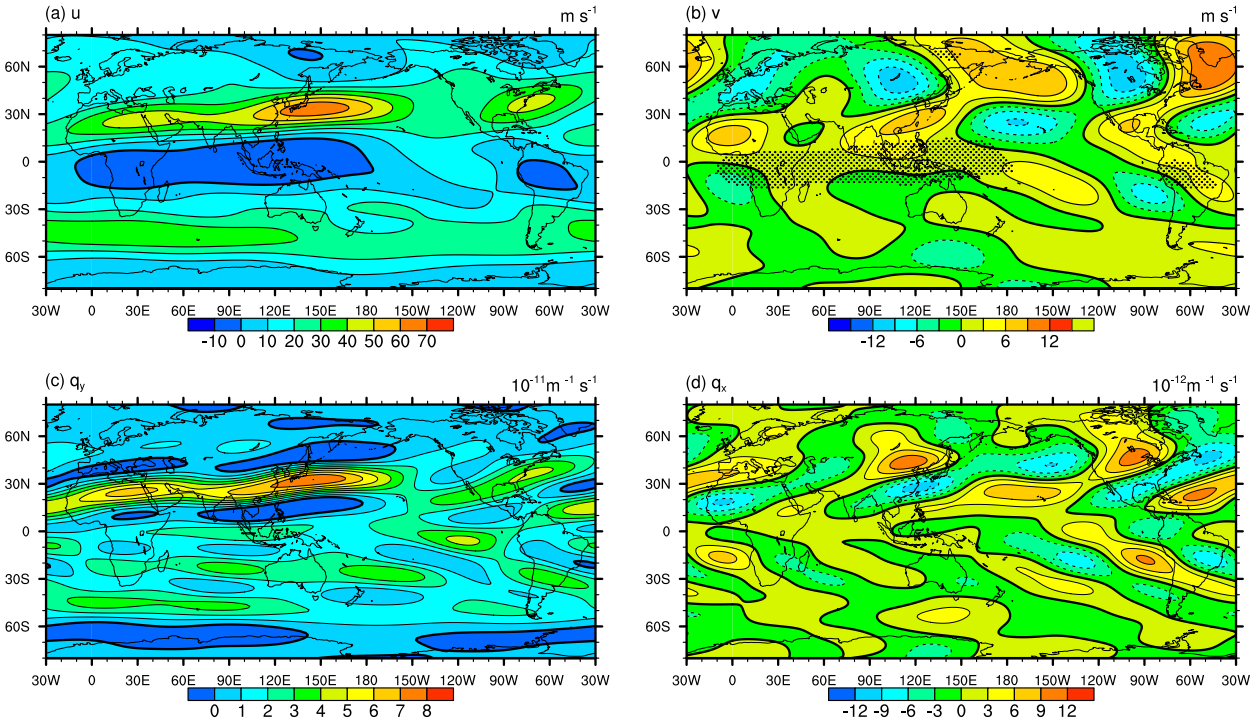

FIG. 4. The 250-hPa climatology of (a) zonal wind, (b) meridional wind, (c) meridional gradient of absolute vorticity, and (d) zonal gradient of absolute vorticity based on ERA-40. Contour intervals are $10\,m\,s^{-1}$, $3\,m\,s^{-1}$, $10^{-11}\,m^{-1}\,s^{-1}$, and $10^{-12}\,m^{-1}\,s^{-1}$ in (a)–(d), respectively. The dotted regions in (b) denote the climatological easterlies.

stationary Rossby wave propagation behavior. Based on the theoretical analysis in section 4, the basic flow determines the propagation behavior. For ZVZF, we only show the positive propagating meridional wavenumber (northward), as the other propagating solution is just the opposite (southward) from Eq. (7). For PHNF or FHNF, there are three propagating wave roots for situations where Eq. (12) is satisfied and one propagating wave root elsewhere. Figure 5 shows the number of propagating wave solutions for ZVZF, PHNF, and FHNF. For PHNF and FHNF, the three-root situation usually occurs near the westerly jet or near zero meridional wind lines. The differences between PHNF and FHNF are minor, especially for small zonal scales (Fig. 5). We examined the behavior of the three roots and found that two are opposite in sign, and the third has a short wavelength ($<10^3$ km). In a local state with three solutions, we only show the two opposite roots with longer wavelengths, as their wave scales are comparable with the meridional scale of the observed circulation anomalies.

Figure 6 shows the propagating meridional wavenumber and the corresponding meridional group velocity for zonal wavenumber 1 calculated for ZVZF and PHNF. With ZVZF, the band of easterlies in the tropics makes it difficult for stationary Rossby waves to propagate across the critical latitudes, whereas the westerly duct region in the eastern equatorial Pacific and equatorial Atlantic favors the north–south bidirectional propagation of shorter waves (Figs. 6a,b), consistent with previous studies (HA).

Introducing the meridional basic flow permitted stationary wave propagation in additional regions. There exists one propagating solution near the critical latitudes, as theory suggested in section 4b. The southerlies in East Africa, the western Indian Ocean, and South Asia act as ducts for northward energy propagation across the easterly layer by Rossby waves with meridional wavenumbers 5–8 (meridional wavelength of 8000–5000 km) and a meridional group velocity of about $5–20\,m\,s^{-1}$, but act as barriers to the southward propagation of energy (Figs. 6c–f). It is worth reminding the reader that the wave solution with negative l is also indicative of northward propagation in the negative $\overline{q}_y$ region at about 10°N (Figs. 4c and 6e–f), according to the theory in section 4b. On the contrary, the northerlies in southwest Africa, the SH tropical Atlantic, and the SH tropical eastern Indian Ocean support southward energy propagation by stationary waves (Figs. 6e,f). For zonal wavenumber 3, the wave propagation behavior through easterly flow is similar to that of zonal wavenumber 1, but with a shorter

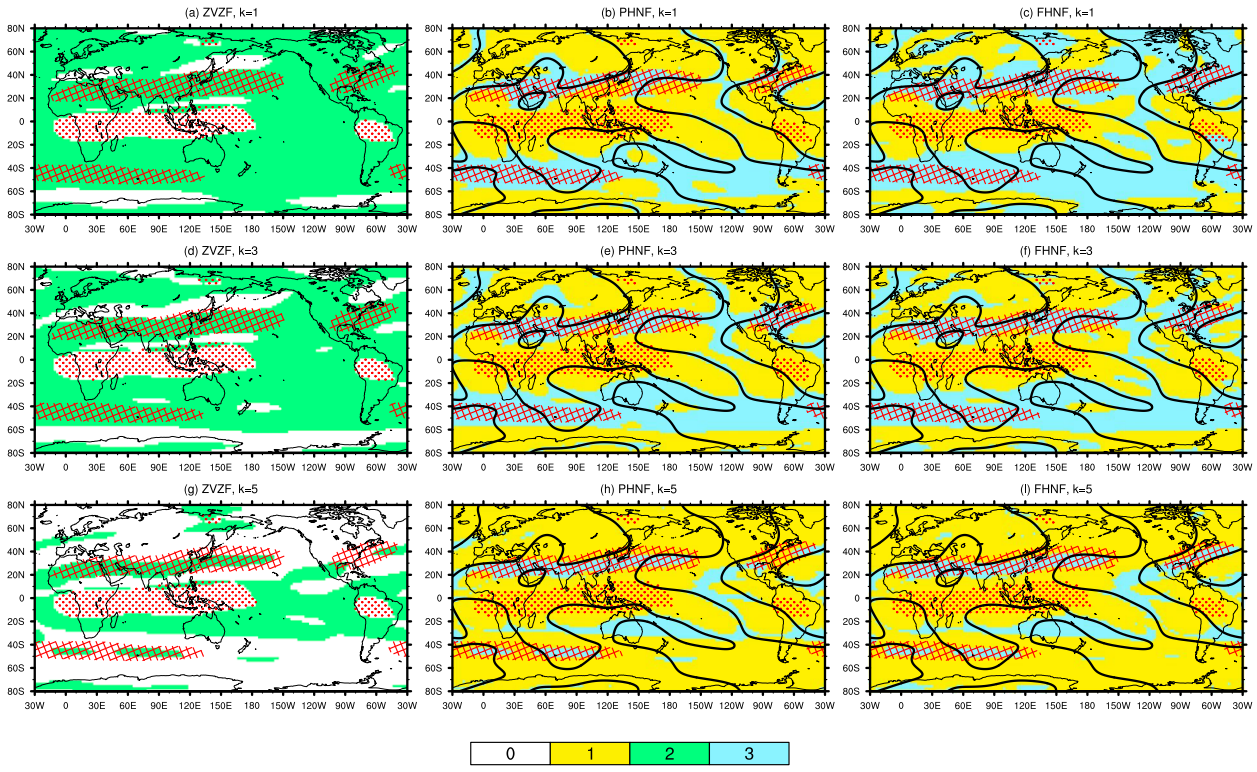

FIG. 5. Number of propagating stationary wave solutions for (top) zonal wavenumbers 1, (middle) 3, and (bottom) 5 for (left) ZVZF, (center) PHNF, and (right) FHNF. The red dotted and hatched regions denote the climatological easterlies ($\overline{u} < 0\,\mathrm{m\,s^{-1}}$) and the westerly jet ($\overline{u} > 30\,\mathrm{m\,s^{-1}}$), respectively. In the PHNF and FHNF panels, thick black lines indicate the climatological zero meridional wind line.

meridional wavelength and a reduced meridional group velocity (Figs. 7c,d).

When the zonal variation of basic flow is included in $\overline{q}_y$ and $\overline{q}_x$ (i.e., in FHNF), the results (see Fig. S5 in the supplemental material) resemble the interhemispheric propagation behavior for PHNF (Fig. 8), indicating that the impact of the meridional basic flow on stationary wave interhemispheric propagation is more important.

The effect of the meridional basic flow on the cross-equatorial propagation in the tropical westerly duct is obvious from Figs. 6 and 7. The eastern equatorial Pacific favors southward propagation, whereas the equatorial Atlantic favors northward propagation (Figs. 6d,f) for zonal wavenumber 1, and thus differs from the north–south bidirectional waveguides on ZVZF. For zonal wavenumber 3, the eastern equatorial Pacific also allows northward propagation and the equatorial Atlantic westerly duct allows southward transmission, which indicates that the westerly duct acts as a two-way north–south waveguide for shorter waves. It is also noted that stationary wave propagation in mid- and high latitudes is strongly influenced by the meridional basic flow. One-way meridional energy propagation dominates the NH mid- and high latitudes (north of 40°N; Figs. 6d,f). For example, northward propagation is favored over the North Pacific and North Atlantic, whereas southward propagation is favored over Eurasia and North America but with a weaker meridional group velocity. These characteristics may be related to meridional dipole low-frequency teleconnections, such as the PNA in the North Pacific and the North Atlantic Oscillation in the North Atlantic. We intend to investigate this hypothesis in another paper.

c. *Wave ray tracing*

The above results from stationary wavenumber and group velocity analysis show that the southerly duct embedded in eastern Africa, the western Indian Ocean, and South Asia favors the northward propagation of stationary waves, and the northerly duct in southwest Africa, the SH tropical Atlantic, and the SH tropical eastern Indian Ocean favors the southward propagation of stationary waves. How then do the waves propagate across the easterly flow to the NH midlatitudes and SH? To answer this question, rays were traced in the two-dimensional nonuniform DJF climatological ambient flow by numerical integration of Eqs. (11) and (12) for 35 days, initiated with a given integer zonal wavenumber at certain forcing sites within the tropical easterlies (15°S–5°N,

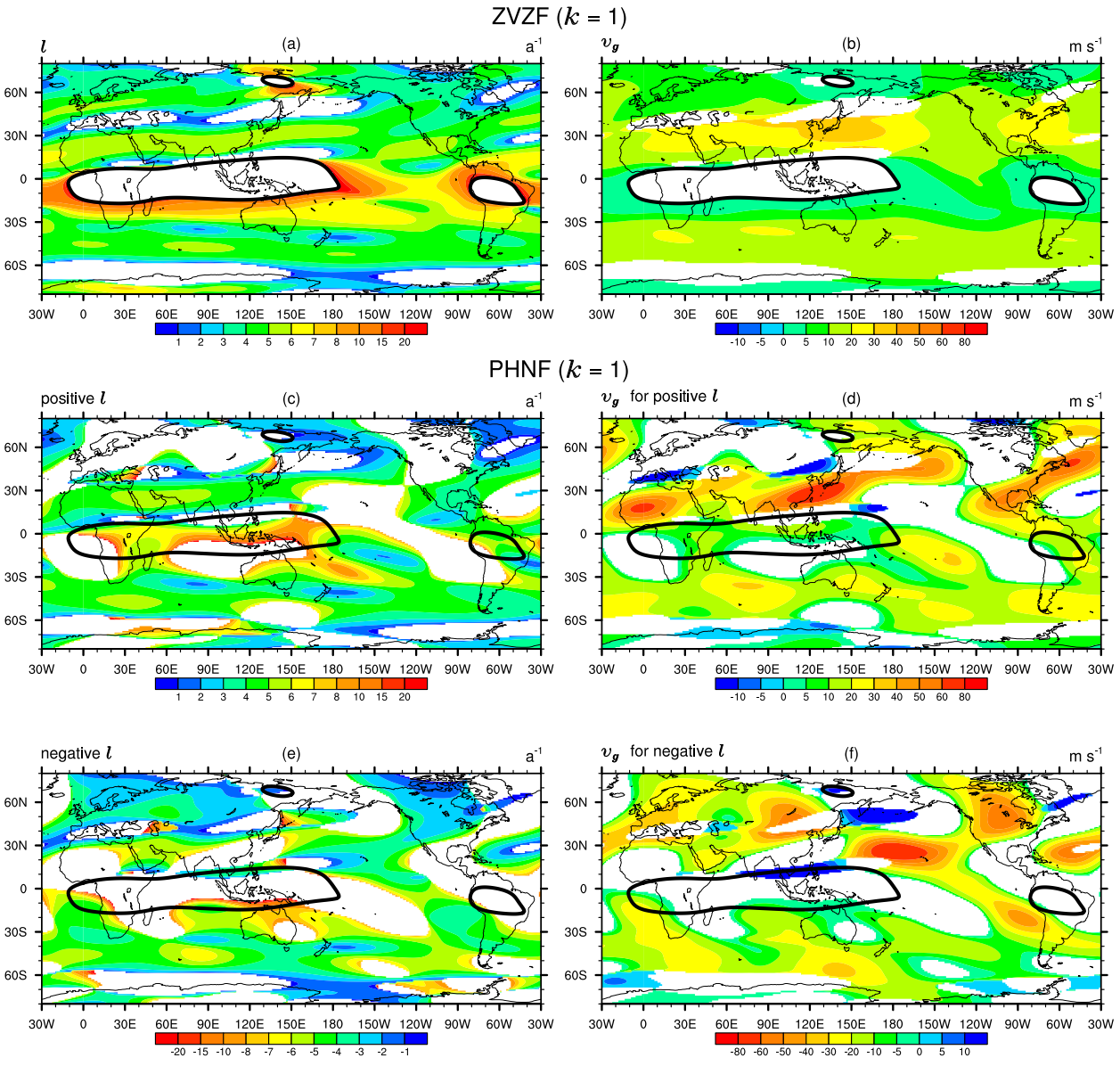

FIG. 6. (left) The propagating local meridional wavenumber solutions of the dispersion relation for stationary waves (units are a^{-1}, where a is the radius of the earth) and (right) the corresponding meridional group velocity (m s^{-1}) with zonal wavenumber 1 on (a),(b) ZVZF, and (c)–(f) PHNF for the (c),(d) positive and (e),(f) negative roots, respectively. Thick black curves denote the climatological zero zonal wind line.

20°–60°E). The initial local meridional wavenumber l is determined from the dispersion relationship in Eq. (13) by assuming $\omega = 0$ (stationary waves) and the given zonal wavenumber. The integrations for the ray paths were terminated when the local meridional wavelength became too short (<1000 km in our numerical calculations) to be comparable with the meridional scale of the observed circulation anomalies.

Figure 8 illustrates the stationary wave ray paths of zonal wavenumbers 1–3 in the FHNF. Only one propagating wave arises from a source in the easterlies (Fig. 5). The stationary wave packets that initiated in the southern African and western Indian Ocean easterlies first propagate westward and northward and are divided into southern and northern branches by the meridional basic flow: that is, the northerly flow in western Africa and the southerly flow over the SH tropical Atlantic. The northern branch propagates northward across the critical latitude into the North African–Asian jet and continues to spread quickly from North Africa, through South Asia to the North Pacific near the date line. Some of these wave packets propagate

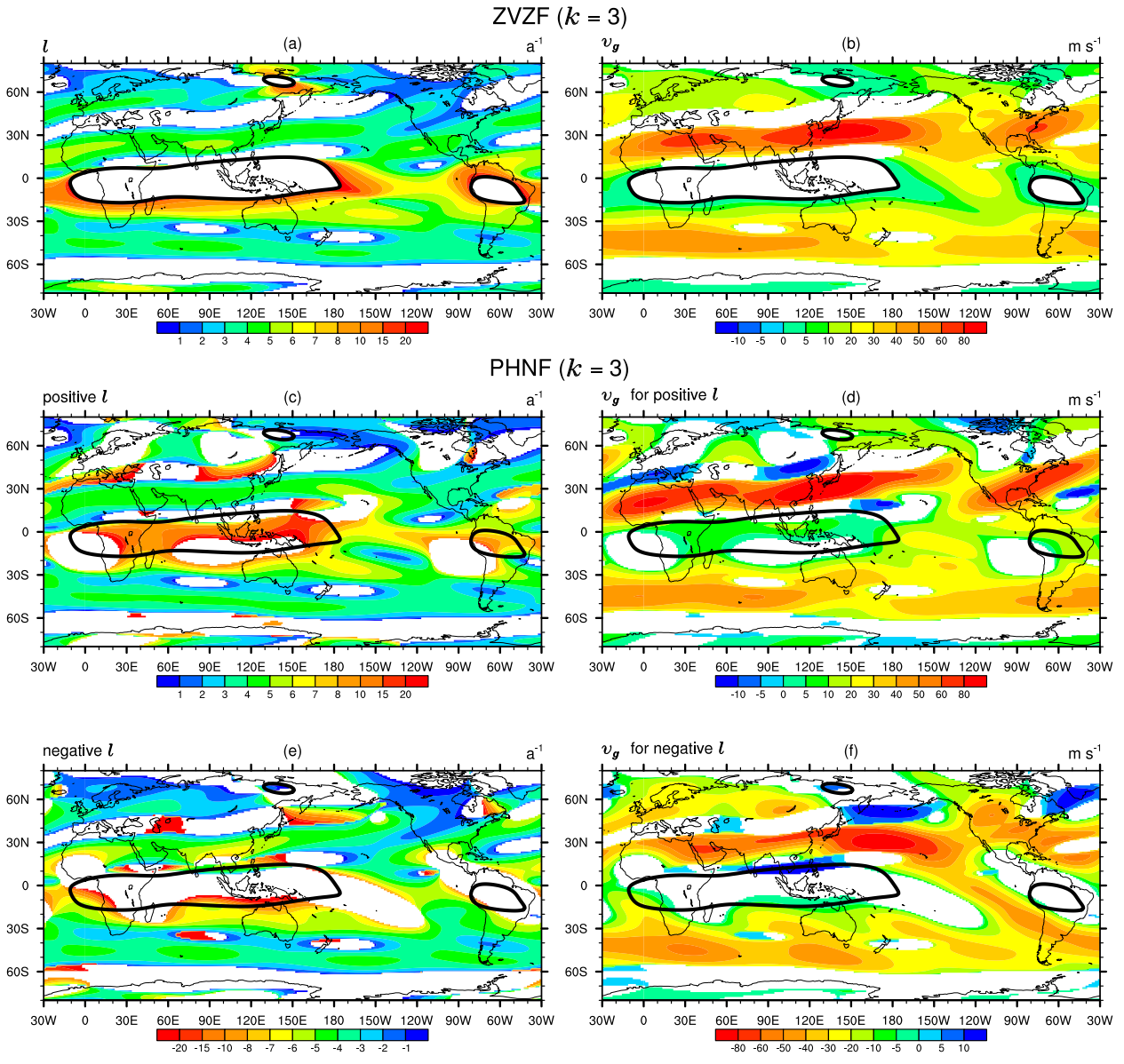

FIG. 7. As in Fig. 6, but for zonal wavenumber 3.

northward to North America following a great circle-like route (Fig. 8a) and may be responsible for the significant anomalies associated with the AAP in the North Pacific. Other wave packets propagate southward to the eastern equatorial Pacific westerly duct, refract to the North American jet (Fig. 8a), or cross the equator into the SH (Figs. 8b,c). The southern branch propagates southward in the SH with one arm extending into the SH midlatitudes and the other propagating eastward at 30°S. These ray tracing results are consistent with the structure of the AAP teleconnection. An examination of ray tracings originating over the SH western Indian Ocean on PHNF yields similar northward propagation behavior to that shown in Fig. 8, indicating the dominant role of meridional flow on interhemispheric propagation.

d. Barotropic model experiments

To further understand the critical influence of a meridional basic flow on interhemispheric wave propagation across the critical latitude, we studied the streamfunction responses to forcings in the NH and SH, using a barotropic model linearized about ZVZF and HNF. An examination of forcings centered at the northern and southern tropical Indian Ocean (20°S–20°N, 40°–100°E) yields similar cross-equatorial

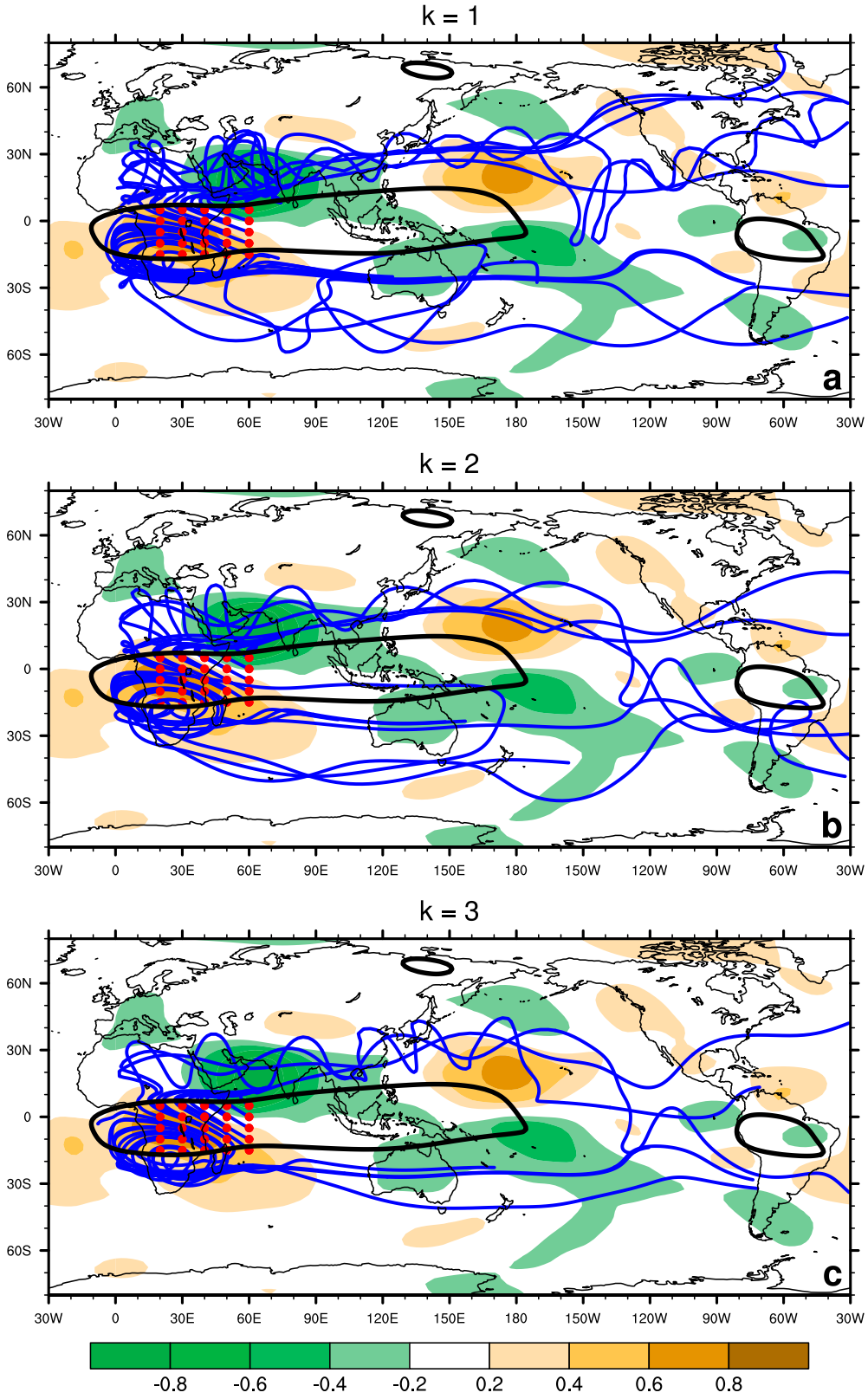

FIG. 8. Stationary Rossby wave ray tracing initiated with zonal wavenumbers (a) 1, (b) 2, and (c) 3 integrated for 35 days on FHNF. Rays (blue lines) start from a source matrix (15°S–5°N, 30°–70°E) denoted by red points. Plots of the ray paths are superimposed on the correlation map between eddy streamfunction and AAPI. Thick black curves denote the climatological zero zonal wind line.

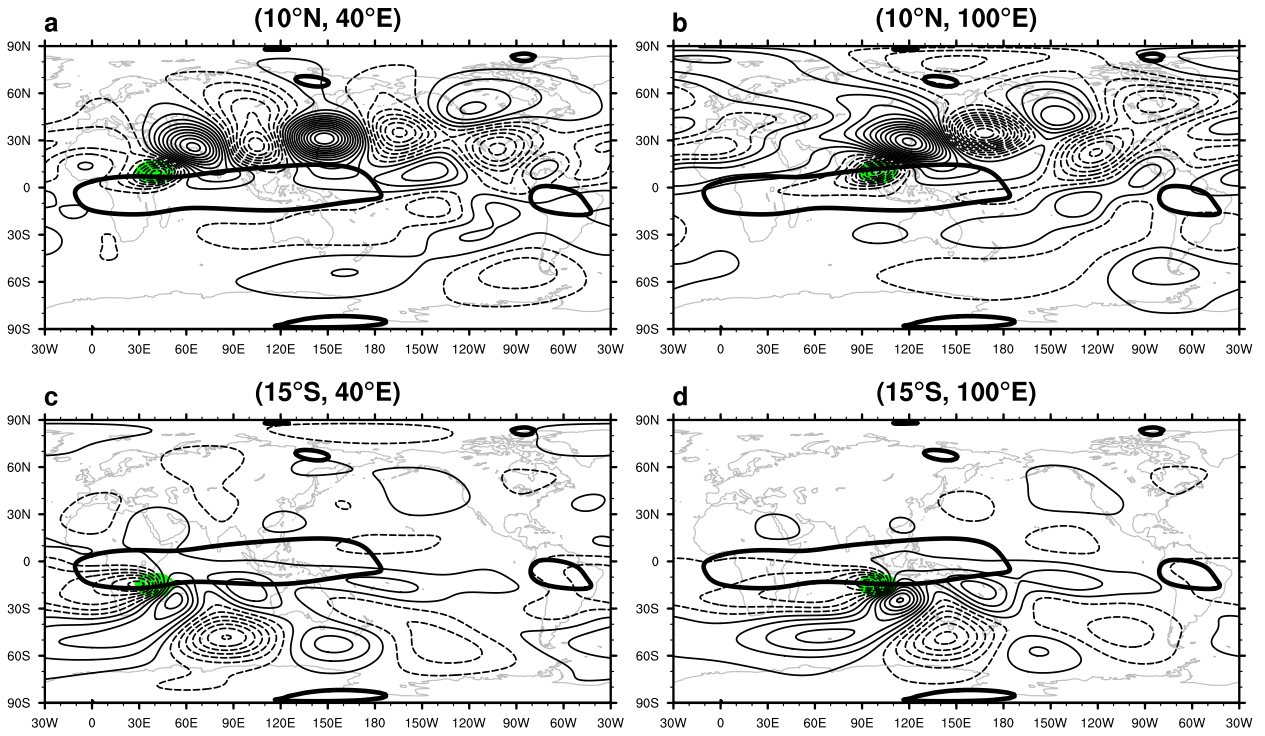

FIG. 9. Steady streamfunction responses (with zonal mean subtracted) to forcing (green shading) located at (a) 10°N, 40°E; (b) 10°S, 100°E; (c) 15°S, 40°E; and (d) 15°S, 100°E on ZVZF derived from the DJF 250-hPa wind climatology. Contours are drawn for ±0.4, ±1.2, ±2.0, 2.8, ... × 10^6 m^2 s^{-1}, with negative contours dashed. Thick black curves denote the zero zonal wind line.

propagation characteristics. For brevity, the NH forcing is shown at 10°N, 40°E and 10°N, 100°E, and the SH forcing is shown at 15°S, 40°E and 15°S, 100°E.

The results of the experiments on ZVZF are illustrated in Fig. 9. With the forcing centered at 10°N, 40°E and 10°N, 100°E, we see that almost all of the energy is trapped in the NH, except for the cross-equatorial propagation of waves in the westerly duct in the eastern equatorial Pacific (Figs. 9a,b). With the forcing centered at 15°S, 40°E and 15°S, 100°E, there is no obvious interhemispheric response in the NH. These solutions agree with wavenumber analysis (Figs. 6a,b and 7a,b) that shows stationary waves cannot propagate across the easterlies in a basic state excluding meridional flow.

Figures 10a–d shows the results of experiments with the same forcings as in Fig. 9, but with the meridional basic flow included in the basic state (i.e., on HNF). The interhemispheric responses to the NH forcings (Figs. 10a,b) are weak and are similar to those for ZVZF (cf. Figs. 9a,b) except for small changes in amplitude. The southward cross-equatorial propagation is only evident in the tropical westerlies in the eastern Pacific and Atlantic, which is in agreement with Figs. 6e,f and 7e,f. However, there are strong interhemispheric responses in the NH to SH forcings (Figs. 10c,d) compared with those for ZVZF (cf. Figs. 9c,d). In particular, strong cross-equatorial propagation is evident in the longitudinal band at about 150°E–120°W (Fig. 10c) and in the longitudinal band at about 80°–20°W (Fig. 10d), caused by the northerlies in the basic state (Fig. 4b). This interpretation is consistent with the propagating wave analysis (Fig. 7c,d).

There is also a northward wave path into the North African–Asian subtropical jet in eastern Africa, the western Indian Ocean, and South Asia (Figs. 6c,d and 8). However, the steady responses might be affected by the superposition of wave trains that propagate across the equator through the westerly duct (Figs. 10c,d). To address this issue more directly, the experiments were repeated with an HNF basic state (Figs. 10e–h), which was artificially modified to prohibit interhemispheric wave propagation in the longitudinal band 150°E–0° in the Western Hemisphere (WH). This prohibition is achieved by replacing the zonal wind in the zonal band 20°S–10°N with the zonal mean of the EH (0°–150°E) and setting the meridional wind of the tropical WH (150°E–0°, 30°S–30°N) to zero. Thus, easterly winds prevail over the entire zonal band 20°S–10°N, and there is no meridional flow in the tropical WH in the modified HNF basic state (see Fig. S6 in the supplemental material). This makes it difficult for stationary waves to propagate across the equator in the tropical WH. As shown in Figs. 10e–f, the interhemispheric responses to

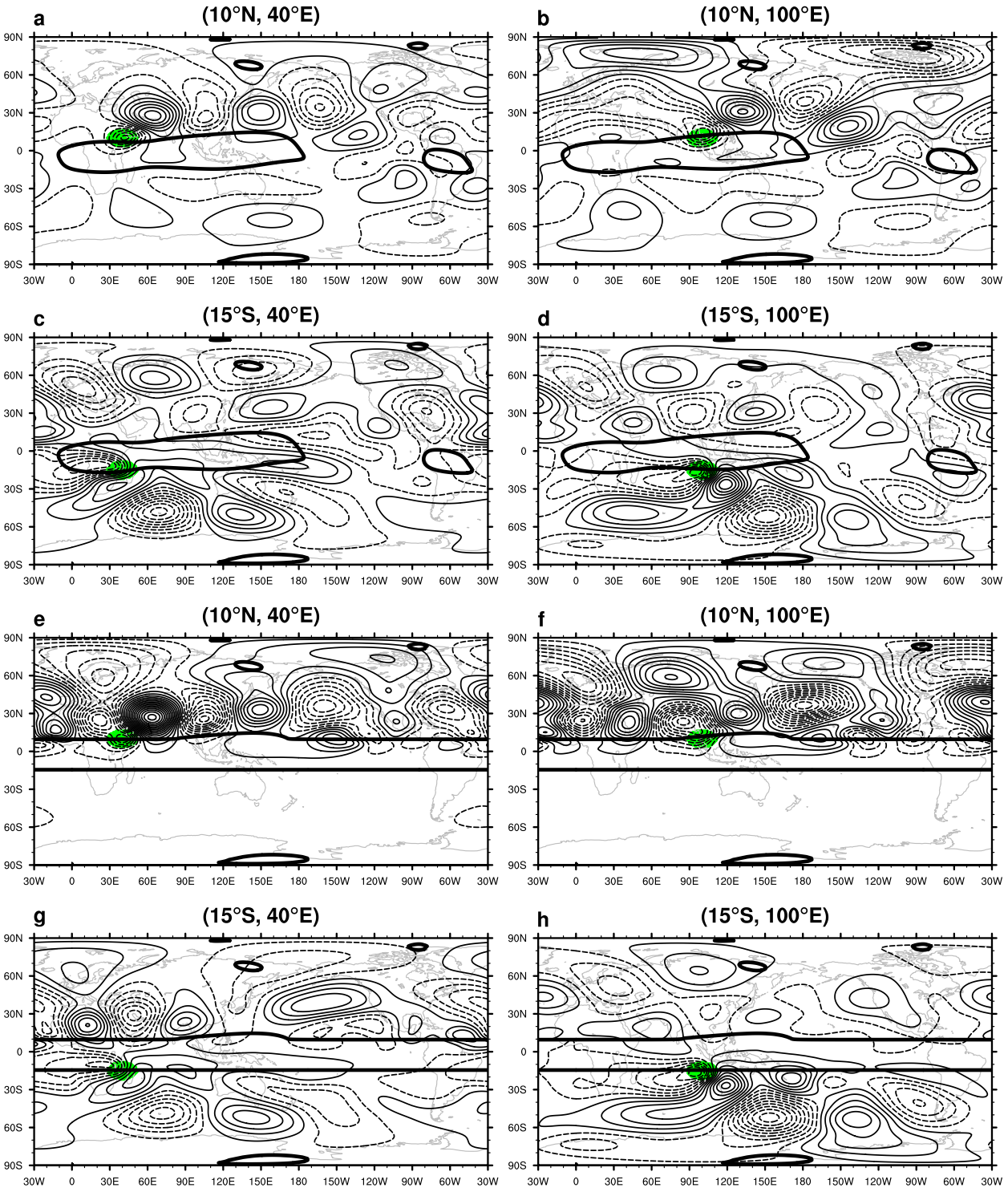

FIG. 10. As in Fig. 9, but (a)–(d) for HNF and (e)–(h) for the modified HNF (see text for details).

NH forcings are no longer evident (cf. Figs. 10c,d). Conversely, the responses to the SH forcings at 15°S, 40°E and 15°S, 100°E clearly exhibit wavelike patterns northward across the critical latitude in the southerly duct in northern Africa and the western Indian Ocean (Figs. 10g,f), which are in agreement with Figs. 6c,d and 7c,d. The experiments regarding forcing at various other locations in the southern tropical Indian Ocean

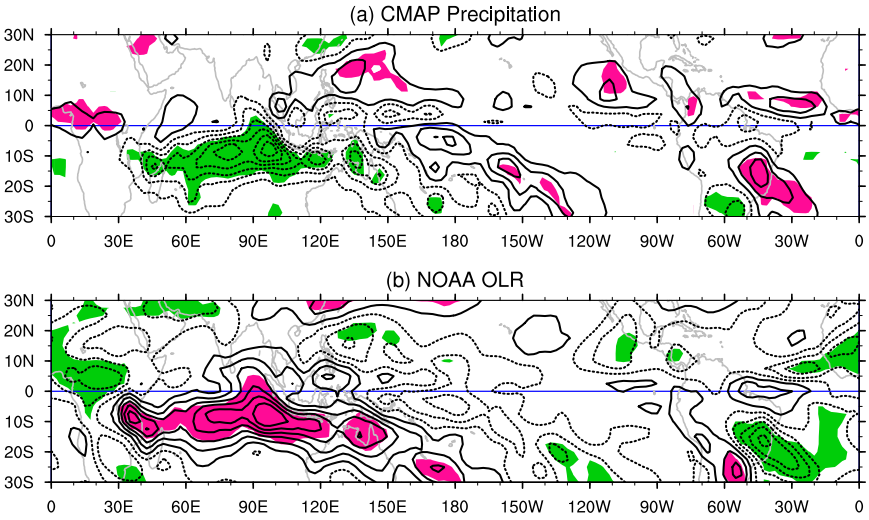

FIG. 11. Regression maps of (a) CMAP precipitation and (b) OLR for the AAPI after removal of the contributions of SEA, EU, PNA, and WP teleconnections and ENSO. Precipitation contours are drawn for ±0.25, ±0.75, ±1.25, ... mm day^{-1}, and OLR contours are plotted for ±1, ±3, ±5, ... W m^{-2} with negative contours dotted The shaded areas indicate significance at the 99% confidence level (Student's *t* test).

also support the idea that the southerly duct in eastern Africa, the western Indian Ocean, and South Asia favors the northward propagation of waves into the NH.

6. Discussion and conclusions

This study examined the interhemispheric teleconnections of the 250-hPa streamfunction field during the boreal winter months through teleconnectivity analysis. We found that both the NCEP–NCAR and ERA-40 data exhibit a teleconnection (the AAP pattern) across the critical latitude from southern Africa through South Asia to the North Pacific. Further partial correlation analysis suggests that the AAP teleconnection pattern is likely to be independent of the well-known teleconnections (such as the EU, SEA, PNA, and WP) and is not forced by ENSO.

To reveal the underlying mechanisms responsible for the interhemispheric AAP teleconnection across the critical latitude, we reviewed stationary Rossby wave propagation theory on ZVZF and HNF and theoretically discussed the propagation behavior across the critical latitude, taking account of the meridional ambient flow. Theoretical discussion has shown that the meridional ambient flow can locally open up a path for one-way propagation of stationary waves across the critical latitude and that the meridional propagation direction of the wave is always the same as the meridional basic flow. Stationary wavenumber and group velocity analysis, ray tracing techniques, and simple barotropic model experiments confirm that southerly flow over eastern Africa, the western Indian Ocean, and South Asia favors the northward propagation of stationary waves across the critical latitude to the NH and that these waves are consistent with the structure of the AAP teleconnection. An approximation to the basic state, PHNF, is shown to be valid for propagation near the critical latitudes. That is, the variations in meridional flow are small terms in the basic-state absolute vorticity gradient and can be ignored when investigating the effect of meridional flow on the interhemispheric propagation of energy.

Previous observational studies have shown an AAP-like pattern in the upper troposphere on intraseasonal and interannual time scales [Hsu and Lin 1992 (their Figs. 4a,b); Branstator 2002 (his Fig. 12b); Matthews et al. 2004 (their Fig. 1)] during the boreal winter. Matthews et al. (2004) inferred these circulation anomalies to be forced by a tropical forcing with the main body located in the SH (their Fig. 3a), based on numerical model experiments. As shown in Fig. 11, the positive (negative) phase of the AAP teleconnection is associated with below- (above-) normal convective activity over the southern tropical Indian Ocean, indicating the AAP teleconnection could be driven by anomalous heating in this region.

However, Matthews et al. (2004) failed to explain why the extratropical anomalies in the NH are stronger than those in the SH. A number of experiments with the forcing in different latitudes have been designed with the linear baroclinic model linearized about DJF 3D climatology (see appendix for details). The modeled response to the heating sink centered in the southern tropical Indian Ocean (Figs. 12a,b) is very similar to the

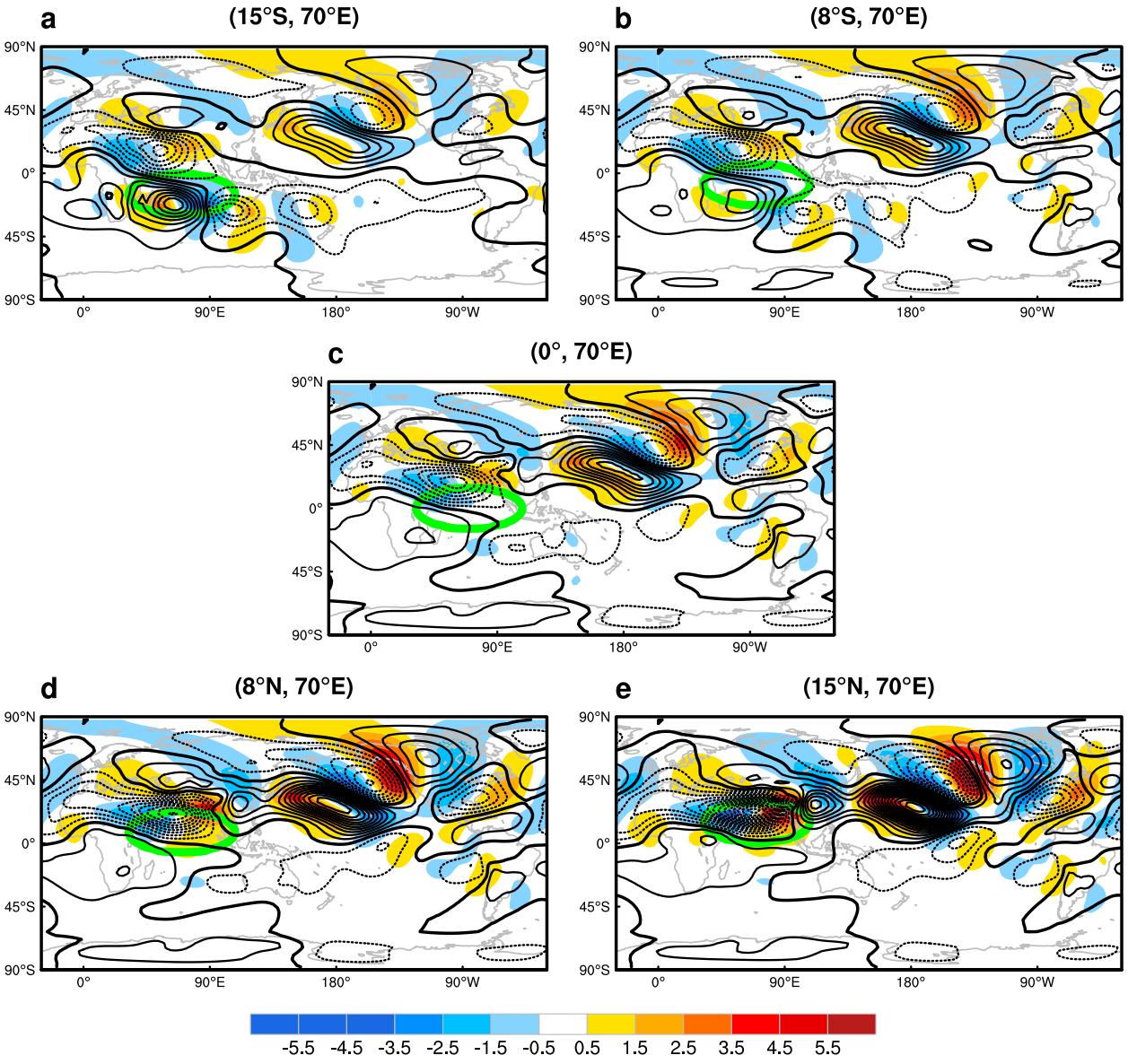

FIG. 12. Steady 250-hPa streamfunction (contours) and meridional wind (shading) response to the tropical Indian Ocean heating sinks in the linear baroclinic model linearized about the 3D DJF climatology. The heating sinks are centered at (a) 15°S, (b) 8°S, (c) equator, (d) 8°N, and (e) 15°N along the same longitude 70°E. The nonzero heating regions are indicated by green lines. The contour interval is $10^6\,m^2\,s^{-1}$, with negative contours dotted and zero contours thickened.

observed AAP teleconnection, except that the quadrupole feathers in the SH lie east of the observations. This shift is thought to be generated by the unrealistic strength of damping of the model dynamical fields (Matthews et al. 2004). Furthermore, the prescribed forcing is a simplification of the real atmosphere (Fig. 11) and is unable to reproduce the exact shape. Nevertheless, comparison of Figs. 12a,b with Figs. 12d,e shows that the southern heating sink can force strong anomalies in the NH, whereas NH forcing cannot generate comparative anomalies in the SH. The meridional wind responses to southern heating sinks clearly demonstrate the pathway of northward energy dispersion (Figs. 12a,b), consistent with wave ray tracing (Fig. 8) and thus supporting the hypothesis that northward propagation of stationary waves across the critical latitude affects the NH extratropical anomalies of the AAP teleconnection.

The different interhemispheric teleconnections may involve several mechanisms. Some patterns may result from sources within the tropical easterlies that excite a midlatitude response in both hemispheres. Instead, our theoretical analysis and model experiments raise the

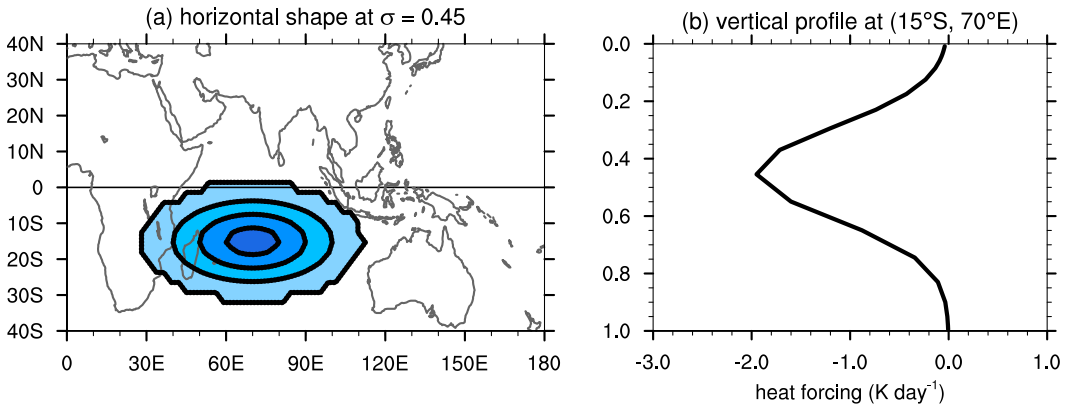

FIG. A1. (a) Horizontal distribution (at the sigma level = 0.45) and (b) vertical profile of the specific center at 15°S, 70°E of the heat source.

possibility of the direct propagation of stationary waves through regions of easterlies from one hemisphere to the other. This helps to explain why the observed southern tropical Indian Ocean convective anomalies (Fig. 11) excite the extratropical anomalies in the NH more strongly than those in the SH (Fig. 3). In another work (Li et al. 2015), we also discussed the possibility of stationary waves propagating across the tropical easterly in HNF, but here we consider more configurations of the basic state at the critical latitude from a theoretical perspective and focused on the boreal winter. The present work, together with previous studies, provides insight into interhemispheric teleconnections.

It is argued that nonlinearity becomes important for stationary Rossby waves close to the critical latitude in the zonally varying basic flow (Killworth and McIntyre 1985; Haynes 1985). Magnusdottir and Haynes (1999) and Abatzoglou and Magnusdottir (2004) demonstrated absorption–reflection behavior in the neighborhood of the critical latitude; however, the nonlinear behavior around the critical latitude on HNF is less clear. Therefore, further analysis is needed to clarify this point. Nathan and Hodyss (2010) derived an extended Charney–Drazin condition for zonally nonuniform background flow and showed that local vertical propagation (trapping) is possible for wave scales for which the traditional Charney–Drazin condition predicts trapping (propagation). The vertical propagation behavior of waves in a more realistic flow is also unclear. Therefore, it would be of interest to perform theoretical analysis and calculations for vertically propagating Rossby waves similar to those presented here so as to analyze troposphere–stratosphere interactions in more realistic flows.

Acknowledgments. We are grateful to Prof. M. Watanabe for making the linear baroclinic model readily available and three anonymous reviewers for their constructive comments and suggestions. This work was jointly sponsored by the National Natural Science Foundation of China (Grants 41030961, 41205034, and 91437216).

APPENDIX

Linear Baroclinic Model

The linear baroclinic model used in this study consists of primitive equations linearized about a 3D DJF climatology obtained from ERA-40 for 1958–2001. The model adopts a horizontal spectral resolution of T42 and has 20 vertical levels with a sigma (σ) coordinate system, and it includes horizontal and vertical diffusion, Rayleigh friction, and Newtonian damping. The horizontal diffusion has a damping time scale of 2 h for the smallest wave, and the Rayleigh friction and Newtonian damping have a time scale of $(0.5\ \text{day})^{-1}$ in the lowest three levels and top one level, $(5\ \text{day})^{-1}$ for the fourth level, and $(30\ \text{day})^{-1}$ between them. Details of the model formulation are given in Watanabe and Kimoto (2000). The prescribed forcing for the dry version of the linear model has a cosine-squared horizontal profile in an elliptical region:

$$Q = \begin{cases} Q_0 \cos^2\left(\dfrac{\lambda-\lambda_0}{\Delta\lambda}\right)\cos^2\left(\dfrac{\varphi-\varphi_0}{\Delta\varphi}\right), & \text{for} \quad |\lambda-\lambda_0| \le \Delta\lambda, |\varphi-\varphi_0| \le \Delta\varphi \\ 0, & \text{otherwise} \end{cases}.$$

The meridional and zonal extent of the heating centered at (λ_0, φ_0) is determined by the half-width $\Delta\varphi$ and $\Delta\lambda$. The vertical profile is a gamma vertical profile with maximum at 400 hPa ($\sigma = 0.45$), basically in agreement with the observed profile of precipitation variability, and has been employed in many previous studies (e.g., Rodwell and Hoskins 1996; Matthews et al. 2004). The maximum heating imposed at 400 hPa is $2\,\mathrm{K\,day^{-1}}$, which is approximately equivalent to $4.0\,\mathrm{mm\,day^{-1}}$ of anomalous precipitation and is thus consistent with Fig. 11. An example of a heating sink centered at 15°S, 70°E is shown in Fig. A1. The zonal and meridional extents of the heating anomalies over the Indian Ocean are 80° and 30°, respectively.

To obtain the linear atmospheric response to forcing, we adopt a time integration method. The integration is continued up to 30 days, and the results averaged for days 26–30 are shown as the steady response to a prescribed diabatic heating forcing. The circulation response approaches the steady state approximately after day 20.

REFERENCES

Abatzoglou, J. T., and G. Magnusdottir, 2004: Nonlinear planetary wave reflection in the troposphere. *Geophys. Res. Lett.*, **31**, L09101, doi:10.1029/2004GL019495.

Ambrizzi, T., B. J. Hoskins, and H. H. Hsu, 1995: Rossby wave propagation and teleconnection patterns in the austral winter. *J. Atmos. Sci.*, **52**, 3661–3672, doi:10.1175/1520-0469(1995)052<3661:RWPATP>2.0.CO;2.

Branstator, G., 1983: Horizontal energy propagation in a barotropic atmosphere with meridional and zonal structure. *J. Atmos. Sci.,* **40**, 1689–1708, doi:10.1175/1520-0469(1983)040<1689:HEPIAB>2.0.CO;2.

——, 1990: Low-frequency patterns induced by stationary waves. *J. Atmos. Sci.*, **47**, 629–648, doi:10.1175/1520-0469(1990)047<0629:LFPIBS>2.0.CO;2.

——, 2002: Circumglobal teleconnections, the jet stream waveguide, and the North Atlantic Oscillation. *J. Climate*, **15**, 1893–1910, doi:10.1175/1520-0442(2002)015<1893:CTTJSW>2.0.CO;2.

CPC, 1995: CPC Merged Analysis of Precipitation (CMAP). NOAA/OAR/ESRL Physical Sciences Division, accessed 1 October 2013. [Available online at http://www.esrl.noaa.gov/psd/data/gridded/data.cmap.html.]

——, 1996: NOAA Interpolated Outgoing Longwave Radiation (OLR). NOAA/OAR/ESRL Physical Sciences Division, accessed 1 October 2013. [Available online at http://www.esrl.noaa.gov/psd/data/gridded/data.interp_OLR.html.]

——, 2011: Monthly atmospheric & SST indices. NOAA Center for Weather and Climate Prediction, accessed 1 October 2013. [Available online at http://www.cpc.ncep.noaa.gov/data/indices/.]

Dettinger, M. D., D. S. Battisti, R. D. Garreaud, G. J. McCabe, and C. M. Bitz, 2001: Interhemispheric effects of interannual and decadal ENSO-like climate variations on the Americas. *Interhemispheric Climate Linkages: Present and Past Climates in the Americas and their Societal Effects*, V. Markgraf, Ed., Academic Press, 1–16, doi:10.1016/B978-012472670-3/50004-5.

Ding, Q., and B. Wang, 2005: Circumglobal teleconnection in the Northern Hemisphere summer. *J. Climate*, **18**, 3483–3505, doi:10.1175/JCLI3473.1.

ECMWF, 2005: ERA40 2.5 degree latitude-longitude gridded surface and single level analysis. ECMWF Public Datasets, accessed 1 October 2013. [Available online at http://apps.ecmwf.int/datasets/.]

Enomoto, T., B. J. Hoskins, and Y. Matsuda, 2003: The formation mechanism of the Bonin high in August. *Quart. J. Roy. Meteor. Soc.*, **129**, 157–178, doi:10.1256/qj.01.211.

Frederiksen, J. S., and P. J. Webster, 1988: Alternative theories of atmospheric teleconnections and low-frequency fluctuations. *Rev. Geophys.*, **26**, 459–494, doi:10.1029/RG026i003p00459.

Haynes, P. H., 1985: Nonlinear instability of a Rossby-wave critical layer. *J. Fluid Mech.*, **161**, 493–511, doi:10.1017/S0022112085003020.

Hines, K. M., and D. H. Bromwich, 2002: A pole to pole west Pacific atmospheric teleconnection during August. *J. Geophys. Res.*, **107**, 4359, doi:10.1029/2001JD001335.

Hoskins, B. J., and D. J. Karoly, 1981: The steady linear response of a spherical atmosphere to thermal and orographic forcing. *J. Atmos. Sci.*, **38**, 1179–1196, doi:10.1175/1520-0469(1981)038<1179:TSLROA>2.0.CO;2.

——, and T. Ambrizzi, 1993: Rossby wave propagation on a realistic longitudinally varying flow. *J. Atmos. Sci.*, **50**, 1661–1671, doi:10.1175/1520-0469(1993)050<1661:RWPOAR>2.0.CO;2.

Hsu, H. H., and S. H. Lin, 1992: Global teleconnections in the 250-mb streamfunction field during the Northern Hemisphere winter. *Mon. Wea. Rev.*, **120**, 1169–1190, doi:10.1175/1520-0493(1992)120<1169:GTITMS>2.0.CO;2.

Ji, X., J. D. Neelin, S. K. Lee, and C. R. Mechoso, 2014: Interhemispheric teleconnections from tropical heat sources in intermediate and simple models. *J. Climate*, **27**, 684–697, doi:10.1175/JCLI-D-13-00017.1.

Kalnay, E., and Coauthors, 1996: The NCEP/NCAR 40-Year Reanalysis Project. *Bull. Amer. Meteor. Soc.*, **77**, 437–471, doi:10.1175/1520-0477(1996)077<0437:TNYRP>2.0.CO;2.

Karoly, D. J., 1983: Rossby wave propagation in a barotropic atmosphere. *Dyn. Atmos. Oceans*, **7**, 111–125, doi:10.1016/0377-0265(83)90013-1.

Kiladis, G. N., and K. M. Weickmann, 1992: Circulation anomalies associated with tropical convection during northern winter. *Mon. Wea. Rev.*, **120**, 1900–1923, doi:10.1175/1520-0493(1992)120<1900:CAAWTC>2.0.CO;2.

Killworth, P. D., and M. E. McIntyre, 1985: Do Rossby-wave critical layers absorb, reflect, or over-reflect. *J. Fluid Mech.*, **161**, 449–492, doi:10.1017/S0022112085003019.

Knippertz, P., 2007: Tropical–extratropical interactions related to upper-level troughs at low latitudes. *Dyn. Atmos. Oceans*, **43**, 36–62, doi:10.1016/j.dynatmoce.2006.06.003.

Kraucunas, I., and D. L. Hartmann, 2007: Tropical stationary waves in a nonlinear shallow-water model with realistic basic states. *J. Atmos. Sci.*, **64**, 2540–2557, doi:10.1175/jas3920.1.

Lee, S.-K., C. R. Mechoso, C. Wang, and J. D. Neelin, 2013: Interhemispheric influence of the northern summer monsoons on southern subtropical anticyclones. *J. Climate*, **26**, 10 193–10 204, doi:10.1175/JCLI-D-13-00106.1.

Li, L., and T. R. Nathan, 1994: The global atmospheric response to low-frequency tropical forcing: Zonally averaged basic states. *J. Atmos. Sci.*, **51**, 3412–3426, doi:10.1175/1520-0469(1994)051<3412:TGARTL>2.0.CO;2.

——, and ——, 1997: Effects of low-frequency tropical forcing on intraseasonal tropical–extratropical interactions. *J. Atmos.*

Sci., **54**, 332–346, doi:10.1175/1520-0469(1997)054<0332:EOLFTF>2.0.CO;2.

Li, Y., and J. Li, 2012: Propagation of planetary waves in the horizontal non-uniform basic flow (in Chinese). *Chin. J. Geophys.*, **55**, 361–371.

——, ——, F. Jin, and S. Zhao, 2015: Interhemispheric propagation of stationary Rossby waves in the horizontally nonuniform background flow. *J. Atmos. Sci.*, doi:10.1175/JAS-D-14-0239.1, in press.

Liebmann, B., and C. A. Smith, 1996: Description of a complete (interpolated) outgoing longwave radiation dataset. *Bull. Amer. Meteor. Soc.*, **77**, 1275–1277.

Lighthill, J., 1978: *Waves in Fluids.* Cambridge University Press, 504 pp.

Lin, H., 2009: Global extratropical response to diabatic heating variability of the Asian summer monsoon. *J. Atmos. Sci.*, **66**, 2697–2713, doi:10.1175/2009jas3008.1.

Liu, G., L. Ji, S. Sun, and Q. Zhang, 2010: An inter-hemispheric teleconnection and a possible mechanism for its formation. *Adv. Atmos. Sci.*, **27**, 629–638, doi:10.1007/s00376-009-8172-x.

Liu, Z., and M. Alexander, 2007: Atmospheric bridge, oceanic tunnel, and global climatic teleconnections. *Rev. Geophys.*, **45**, RG2005, doi:10.1029/2005RG000172.

Lu, R., J.-H. Oh, and B.-J. Kim, 2002: A teleconnection pattern in upper-level meridional wind over the North African and Eurasian continent in summer. *Tellus*, **54A**, 44–55, doi:10.1034/j.1600-0870.2002.00248.x.

Magnusdottir, G., and P. H. Haynes, 1999: Reflection of planetary waves in three-dimensional tropospheric flows. *J. Atmos. Sci.*, **56**, 652–670, doi:10.1175/1520-0469(1999)056<0652:ROPWIT>2.0.CO;2.

Matthews, A. J., B. J. Hoskins, and M. Masutani, 2004: The global response to tropical heating in the Madden-Julian oscillation during the northern winter. *Quart. J. Roy. Meteor. Soc.*, **130**, 1991–2011, doi:10.1256/qj.02.123.

Nan, S., and J. Li, 2003: The relationship between the summer precipitation in the Yangtze River valley and the boreal spring Southern Hemisphere annular mode. *Geophys. Res. Lett.*, **30**, 2266, doi:10.1029/2003GL018381.

——, ——, X. Yuan, and P. Zhao, 2009: Boreal spring Southern Hemisphere Annular Mode, Indian Ocean sea surface temperature, and East Asian summer monsoon. *J. Geophys. Res.*, **114**, D02103, doi:10.1029/2008JD010045.

Nathan, T. R., and D. Hodyss, 2010: Troposphere–stratosphere communication through local vertical waveguides. *Quart. J. Roy. Meteor. Soc.*, **136**, 12–19, doi:10.1002/qj.532.

NCEP, 1996: NCEP/NCAR Reanalysis monthly mean subsets, 1948-continuing. NOAA/OAR/ESRL Physical Sciences Division, accessed 1 October 2013. [Available online at http://www.esrl.noaa.gov/psd/data/gridded/data.ncep.reanalysis.html.]

Opsteegh, J. D., 1982: On the importance of the Hadley circulation for cross equatorial propagation of stationary Rossby waves. *On the Theory and Application of Simple Climate Models to the Problem of Long Range Weather Prediction: Collected Papers Presented at KNMI Workshop*, De Bilt, Netherlands, KNMI, 49–57.

Rodwell, M. J., and B. J. Hoskins, 1996: Monsoons and the dynamics of deserts. *Quart. J. Roy. Meteor. Soc.*, **122**, 1385–1404, doi:10.1002/qj.49712253408.

Rossby, C. G., 1939: Relation between variations in the intensity of the zonal circulation of the atmosphere and the displacements of the semi-permanent centers of action. *J. Mar. Res.*, **2**, 38–55, doi:10.1357/002224039806649023.

Schneider, E. K., and I. G. Watterson, 1984: Stationary Rossby wave propagation through easterly layers. *J. Atmos. Sci.*, **41**, 2069–2083, doi:10.1175/1520-0469(1984)041<2069:SRWPTE>2.0.CO;2.

Song, J., W. Zhou, C. Li, and L. Qi, 2009: Signature of the Antarctic Oscillation in the Northern Hemisphere. *Meteor. Atmos. Phys.*, **105**, 55–67, doi:10.1007/s00703-009-0036-5.

Tomas, R. A., and P. J. Webster, 1994: Horizontal and vertical structure of cross-equatorial wave propagation. *J. Atmos. Sci.*, **51**, 1417–1430, doi:10.1175/1520-0469(1994)051<1417:HAVSOC>2.0.CO;2.

Trenberth, K. E., G. W. Branstator, D. Karoly, A. Kumar, N.-C. Lau, and C. Ropelewski, 1998: Progress during TOGA in understanding and modeling global teleconnections associated with tropical sea surface temperatures. *J. Geophys. Res.*, **103**, 14 291–14 324, doi:10.1029/97JC01444.

Uppala, S. M., and Coauthors, 2005: The ERA-40 Re-Analysis. *Quart. J. Roy. Meteor. Soc.*, **131**, 2961–3012, doi:10.1256/qj.04.176.

Wallace, J. M., and D. S. Gutzler, 1981: Teleconnections in the geopotential height field during the Northern Hemisphere winter. *Mon. Wea. Rev.*, **109**, 784–812, doi:10.1175/1520-0493(1981)109<0784:TITGHF>2.0.CO;2.

Wang, C., S.-K. Lee, and C. R. Mechoso, 2010: Interhemispheric influence of the Atlantic warm pool on the southeastern Pacific. *J. Climate*, **23**, 404–418, doi:10.1175/2009JCLI3127.1.

Wang, Z., C. P. Chang, B. Wang, and F.-F. Jin, 2005: Teleconnections from tropics to northern extratropics through a southerly conveyor. *J. Atmos. Sci.*, **62**, 4057–4070, doi:10.1175/JAS3600.1.

Watanabe, M., and M. Kimoto, 2000: Atmosphere–ocean thermal coupling in the North Atlantic: A positive feedback. *Quart. J. Roy. Meteor. Soc.*, **126**, 3343–3369, doi:10.1002/qj.49712657017; Corrigendum, **127**, 733–734, doi:10.1002/qj.49712757223.

Webster, P. J., and J. R. Holton, 1982: Cross-equatorial response to middle-latitude forcing in a zonally varying basic state. *J. Atmos. Sci.*, **39**, 722–733, doi:10.1175/1520-0469(1982)039<0722:CERTML>2.0.CO;2.

Whitham, G. B., 1960: A note on group velocity. *J. Fluid Mech.*, **9**, 347–352, doi:10.1017/S0022112060001158.

Wu, Z., J. Li, B. Wang, and X. Liu, 2009: Can the Southern Hemisphere annular mode affect China winter monsoon? *J. Geophys. Res.*, **114**, D11107, doi:10.1029/2008JD011501.

Xie, P. P., and P. A. Arkin, 1997: Global precipitation: A 17-year monthly analysis based on gauge observations, satellite estimates, and numerical model outputs. *Bull. Amer. Meteor. Soc.*, **78**, 2539–2558, doi:10.1175/1520-0477(1997)078<2539:GPAYMA>2.0.CO;2.

Xu, H., 2013: Impacts of Southern Eurasian teleconnection pattern and Atlantic–Eurasian teleconnection pattern on the rainfall over China in winter and autumn. Ph.D. thesis, University of Chinese Academy of Sciences, 124 pp.

Yang, G. Y., and B. Hoskins, 1996: Propagation of Rossby waves of nonzero frequency. *J. Atmos. Sci.*, **53**, 2365–2378, doi:10.1175/1520-0469(1996)053<2365:PORWON>2.0.CO;2.

Yeh, T.-C., 1949: On energy dispersion in the atmosphere. *J. Meteor.*, **6**, 1–16, doi:10.1175/1520-0469(1949)006<0001:OEDITA>2.0.CO;2.

Zheng, F., J. Li, R. T. Clark, and H. C. Nnamchi, 2013: Simulation and projection of the Southern Hemisphere annular mode in CMIP5 models. *J. Climate*, **26**, 9860–9879, doi:10.1175/JCLI-D-13-00204.1.